Supporting Information

Structure of Aerosol-OT

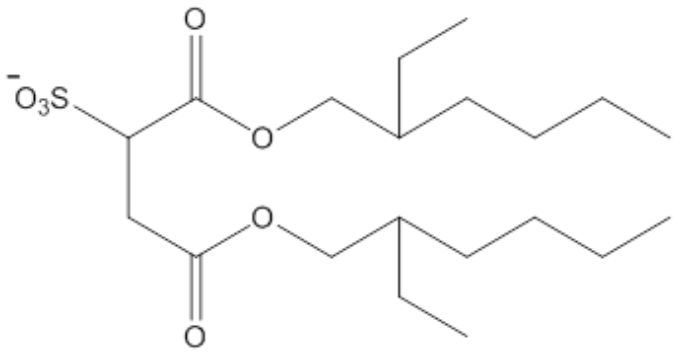

Figure S1. Structure of Aerosol-OT (AOT)

Surfactant Synthesis and Analysis

A saturated aqueous solution (*ca.* 100 cm^3) of cobalt nitrate, (Sigma 98%) was prepared at 25°C and mixed with an ethanolic solution of Na-AOT, 150 cm^3 at 1 mol dm^{-3}. Diethyl ether (50 cm^3) was then added and two phases appeared. The $Co(AOT)_2$ rich organic phase was separated and washed seven times with water (Elga, 18.2 MΩ cm) until clear. The organic solvent was then removed under reduced pressure and residual water removed *in vacuo* at 60 ˚C for 2 days.

The replacement of Na^+ by Co^{2+} was monitored using UV-visible absorbance (Nicolet evolution 300) at A = 510 nm using a range of concentrations (0.01 – 0.10 mol dm^{-3}) of $Co(NO_3)_2$ solutions as standards[1]. The efficiency of the counterion exchange (0.95 ± 0.05) was calculated from the ratio of the observed cation concentration (M^{2+}_{obs}) to the concentration expected (M^{2+}_{ex}) assuming that 1 mol of surfactant contained 1 mol of M^{2+} (*Figure S2*). The divalent ions used bear H_2O ligands, therefore the surfactant is $Co(AOT)_2.6H_2O$.

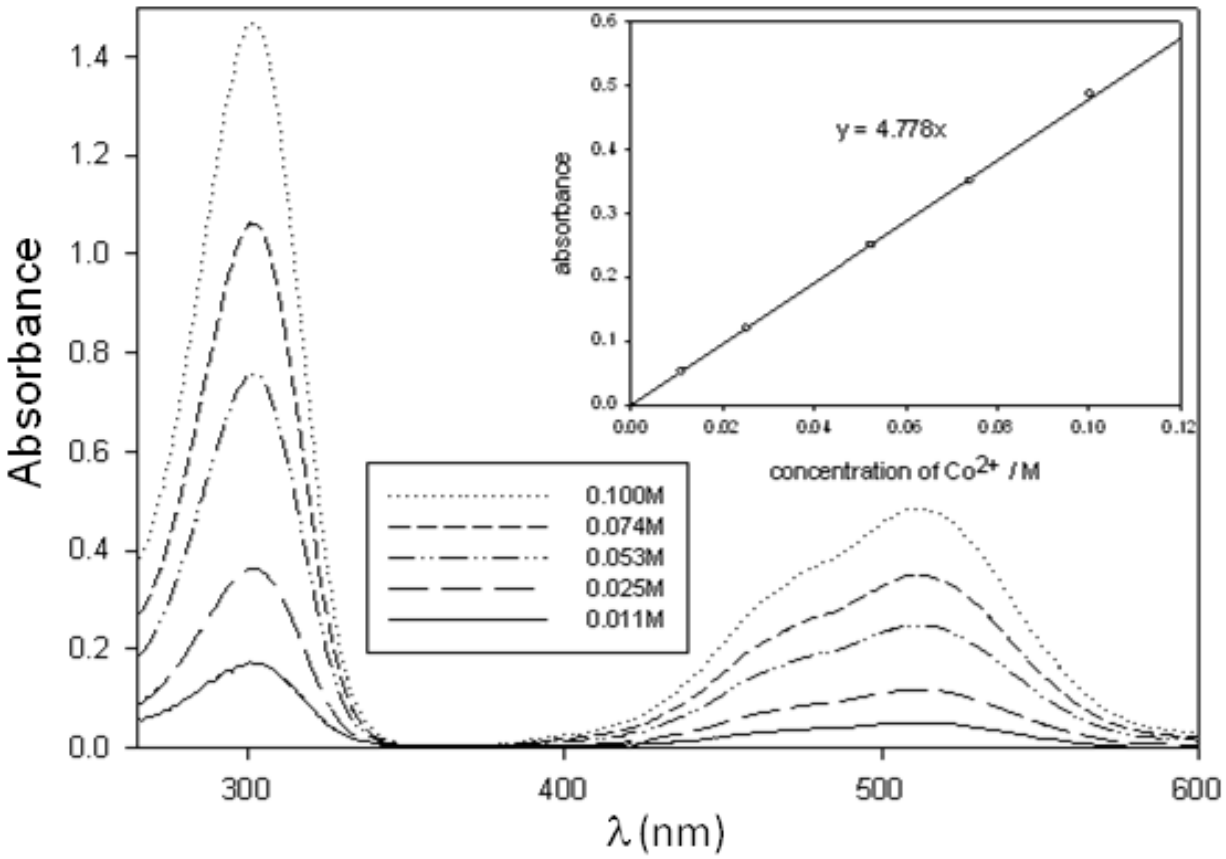

Figure S2: UV-visible absorbance spectra of the $Co(NO_3)_2$ solutions as standards. **Inset:** Beer-Lambert type dependence of absorbance with concentration.

The UV-Visible spectrum for $Co(AOT)_2$ was characteristic of an octahedral complex. The efficiency of the counterion exchange was calculated from the ratio of the observed (Co^{2+}_{obs}) cation concentration to the concentration expected (Co^{2+}_{ex}) assuming that 1 mol of surfactant contained 1 mol of Co^{2+}. The value of $[Co^{2+}]_{obs}/[Co^{2+}]_{ex}$ was 0.95.

The Mn, Ce and Ho AOT analogues were prepared by the liquid-liquid ion exchange process. The appropriate metal chloride (Sigma + 99%) was solubilized in ethanol:H_2O (75:25 v/v). The appropriate equivalent of Na-AOT was then added and the solution stirred for 5 hours. The solvent was then removed under reduced pressure and the metal-surfactant was dried for *in vacuo* at 80°C for two days. The surfactant was then re-solubilized in a minimum amount of dry dicholoromethane and NaCl was filtered off. This was then followed by repeat centrifugation. The pure surfactant was then dried *in vacuo* at 80°C for two days. Analyses showed no chlorine or sodium present and so the synthesis was considered complete.

Polarizing Light Microscopy

The phase progression for Na(AOT) at 25 ˚C agrees with previous work[2]: L_1- L_α- V_2- H_2, where L_1 represents a non-birefringent micellar solution, L_α a lamellar phase with parallel streak patterns, V_2, a non-birefringent cubic bi-continuous phase, and finally, H_2, a fan-like mosaic texture representing a reverse hexagonal phase (Figure S3). In comparison, cobalt and manganese analogues exhibit less varied mesophase structure. Cerium and holmium showed only very limited solubility in water.

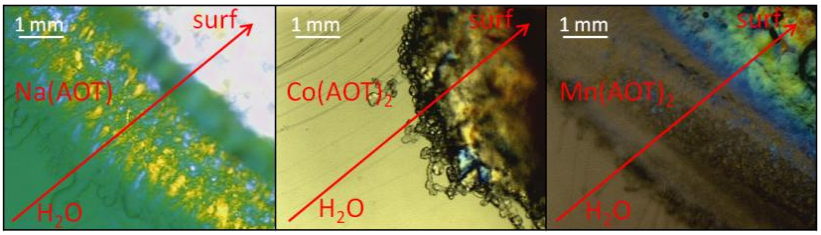

Figure S3: Optical textures of surfactants in water in phase penetration experiments (T = 25 ˚C).

PLM textures show no mesophase formation in heptane; instead only a dilute L_2 phases (inverse micelles) are formed (Figure S4).

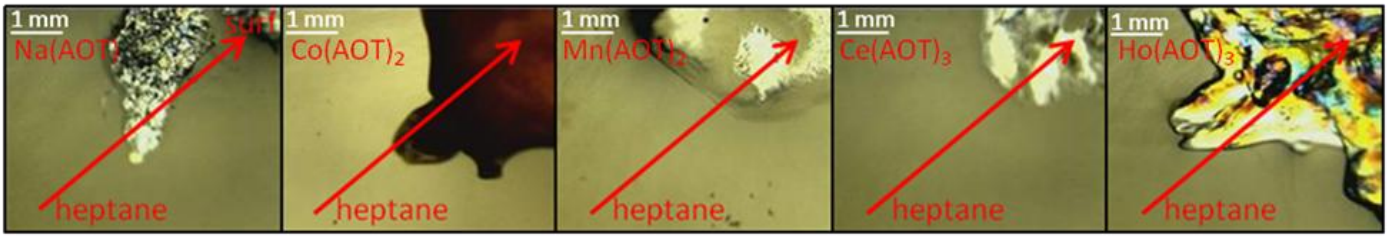

Figure S4: Optical textures of surfactants in heptane in phase penetration experiments (T = 25 ˚C)

SANS Models

The scattered intensity I(Q) has contributions from the size and shape of the aggregates (form factor, P(Q)) and the interaction between aggregates (structure factor, S(Q)),

$$I(Q) \propto P(Q,R)S(Q) \qquad \textbf{Eq. S1}$$

where R is a characteristic particle radius. Data have been fitted with different models using the FISH[3] interactive fitting program, which can be found online (http://www.small-angle.ac.uk).

For water-in-oil microemulsions the main model employed was for a Schultz form factor for polydisperse spheres (P(Q) only).

The model for Na(AOT) in water (D_2O) was an ellipsoidal form factor (P(Q)) multiplied by a Hayter-Penfold charge repulsion S(Q), explicitly declaring molecular fragment sizes and scattering lengths, giving the effective structure factor for charged micelles[4].

The three structural dimensions in the ellipsoidal form factor are the principal radius, R_1, the axial ratio, X, and the secondary radius, R_3. X is 1 for a spherical, < 1 for an oblate and > 1 for a prolate structure.

For S(Q) the value of ϕ is known based on composition and κ^{-1} can be estimated to a first approximation using

$$\kappa = \left(\frac{2F^2\rho I}{\varepsilon_0\varepsilon_r RT}\right)^{1/2} \qquad \textbf{Eq. S2}$$

where F is the Faraday constant, ρ is the solvent density, I the ionic strength, ε_0 is the permittivity of free space and ε_r is the dielectric constant of the solvent. κ^{-1} has the dimensions of length and is a measure of the extent of the electric double layer.

Finally, the SANS profile for $Mn(AOT)_2$ in D_2O was fitted with a form factor for scattering from a thin interface combined with a one dimensional para-crystalline stack model[5]:

$$I(Q) \rightarrow N(\Delta\rho)^2 V^2 \left(\frac{\sin(QL_1/2)}{(QL_1/2)}\right)^2 \qquad \textbf{Eq. S3}$$

With N a concentration in cm^{-3}, $\Delta\rho$ the scattering length difference between solvent and surfactant sheets and L the planar sheet thickness. A modified Lorentz factor allows for a Gaussian distribution of surface normals around the Q vector. The model approximates the local extent of planarity, R^*, the mean layer thickness L, number of layers M, planar spacing D and the Gaussian distribution of L and D as σ_L and σ_D respectively.

SANS Analysis

Na(AOT) forms charged ellipsoidal micelles at 1 wt% in D_2O with a radius of 12 Å and aspect ratio, X = 2.1 (Figure S5). However, the structure in water is concentration dependant with scattering profiles consistent with mixed systems (L_1 + L_α)[6] at higher concentrations. On the other hand, $Co(AOT)_2$ shows a scattering profile consistent with a collapsed lamellar phase, with a Bragg peak at around 31 Å (broadly independent of concentration). Finally, $Mn(AOT)_2$ was fitted to a model for multilamellar stacks[5], with a mean layer thickness of 25 Å and an interlamellar spacing of 58 Å. The SANS from $Mn(AOT)_2$ solutions depends greatly on increasing concentration, becoming more rigid as interbilayer distance decreases.

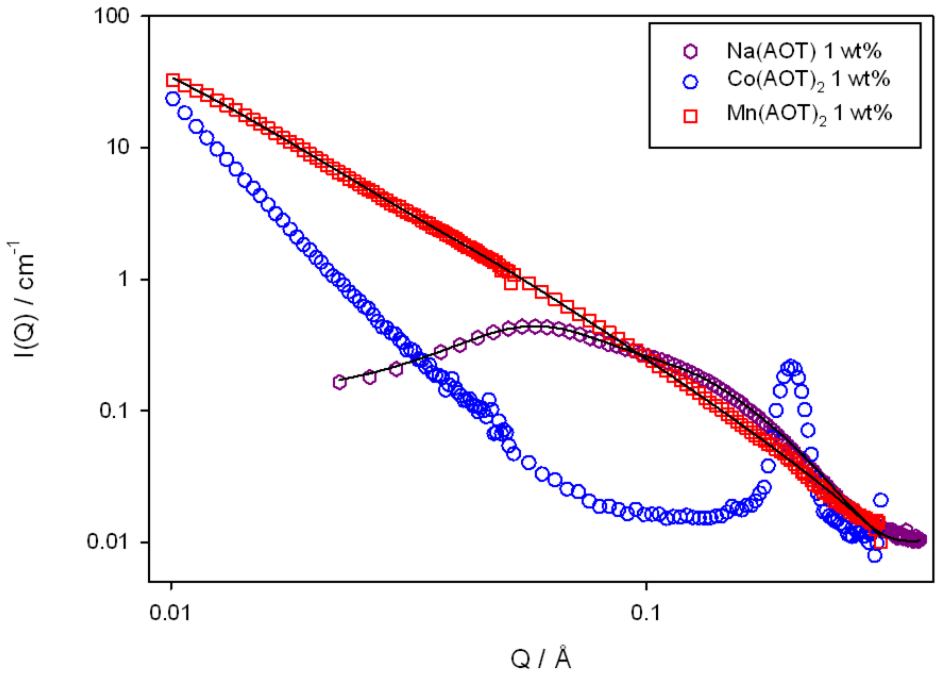

Figure S5: SANS profiles for Na, Co and Mn surfactants in D_2O at 1 wt% at 25 °C.

Lines through the data are fits.

The SANS profiles for the reverse micelles at 1 wt % in heptane could be fitted to Schultz polydisperse spheres with radii between 17 *Å* to 20 *Å (Table S1).* The slight difference in radius is assumed to be the result of the difference in ionic radii of the metal ions combined with different hydration numbers. The cobalt analogue was not soluble above 0.5 wt % but had a structure consistent with literature[7]. An interesting feature of the profiles is the lack any obvious structure factor, (S(Q)), indicating only weak interactions.

Compound	**wt %**	**Radius / *Å***
Na(AOT)	1.0	18
$Co(AOT)_2$	0.5	17
$Mn(AOT)_2$	1.0	20
$Ce(AOT)_3$	1.0	19
$Ho(AOT)_3$	1.0	18

Table S1. Parameters fitted to SANS data from reverse micelles of surfactants using polydisperse sphere model at 1 wt % in n-d_{16}-heptane, 25 ˚C.

Many studies have been undertaken on Na(AOT) w/o microemulsions, showing that it forms discrete spheres regardless of experimental conditions (*e.g.* pressure, temperature, surfactant chain length *etc*.) and that the mean radius of the internal water core, r_c, is directly related to the *w* value.[8] For Na(AOT), $r_c = 1.8w$. For $w = 13.7$ studied here, it should be expected that $r_c = 25$ *Å agreeing with the value elucidated by SANS, $r_c = 26$ Å (Table S2).*

Compound	***w***	**Shape**	**Radius / *Å***
Na(AOT)	13.7	sphere	26 (30)
$Co(AOT)_2$	63.6	sphere	61[a] (57)
$Mn(AOT)_2$	27.8	sphere	25(28)
$Ce(AOT)_3$	24.6	sphere	21(21)
$Ho(AOT)_3$	26.7	sphere	21(22)

Table S2. Parameters fitted to SANS data from w/o microemulsions at 25 ˚C using polydisperse sphere model.

[a]Guinier analysis. Bracketed values from Porod analysis.

Compound	**Mw / (g mol^{-1})**	**χ_m T / (emu K mol^{-1} Oe^{-1})**	**μ_{eff} / (B. M.)**	**θ_p / K**	**T_N / K**
Na(AOT)	**444.25**	**-**	**-**	**-**	**-**
$Co(AOT)_2$	**901.45**	**2.16**	**4.15 (4.20)[a]**	**-4.7**	**20**
$Mn(AOT)_2$	**897.46**	**3.22**	**5.07 (5.92)[a]**	**-6.2**	**60**
$Ce(AOT)_3$	**1403.90**	**0.27**	**1.46 (2.54)[b]**	**-**	**242**
$Ho(AOT)_3$	**1428.71**	**13.61**	**10.43 (10.60)[b]**	**-0.1**	**-**

Table S3. Results derived from SQUID magnetometry. Brackets indicate literature data.

[a]Spin-only moment. [b] Calculated moment.

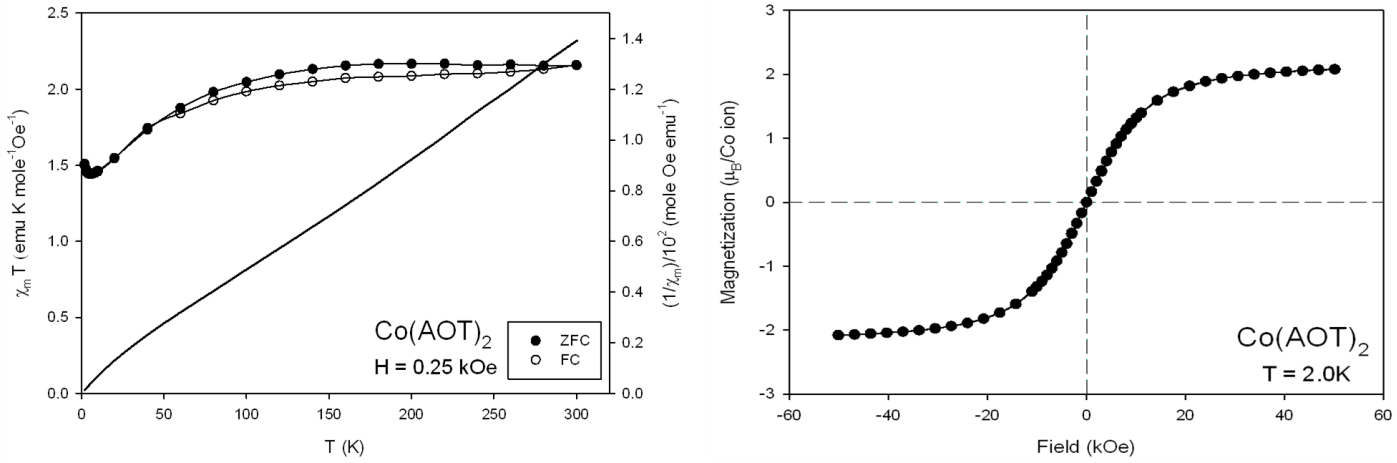

Figure S6a: SQUID magnetometry data for $Co(AOT)_2$ showing **left**: temperature dependence of $\chi_m T$ and $1/\chi_m$ for each surfactant measured under 0.25 kOe; and **right**: magnetization versus applied magnetic field. The inset shows the detail of the low magnetic field region.

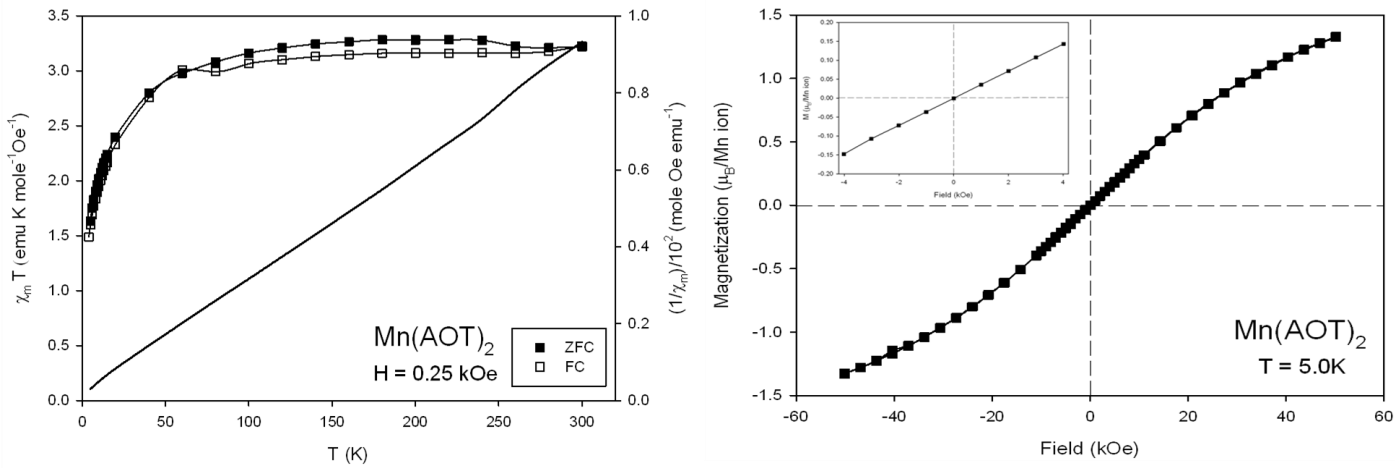

Figure S6b: SQUID magnetometry data for $Mn(AOT)_2$ showing **left**: temperature dependence of $\chi_m T$ and $1/\chi_m$ for each surfactant measured under 0.25 kOe; and **right**: magnetization versus applied magnetic field. The inset shows the detail of the low magnetic field region.

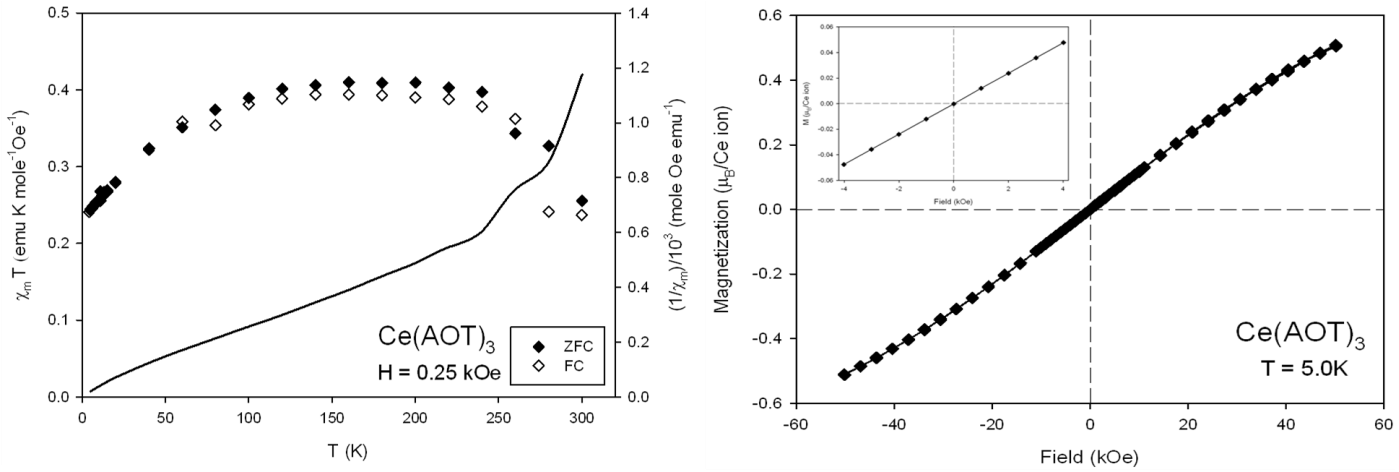

Figure S6c: SQUID magnetometry data for $Ce(AOT)_3$ showing **left**: temperature dependence of $\chi_m T$ and $1/\chi_m$ for each surfactant measured under 0.25 kOe; and **right**: magnetization versus applied magnetic field. The inset shows the detail of the low magnetic field region.

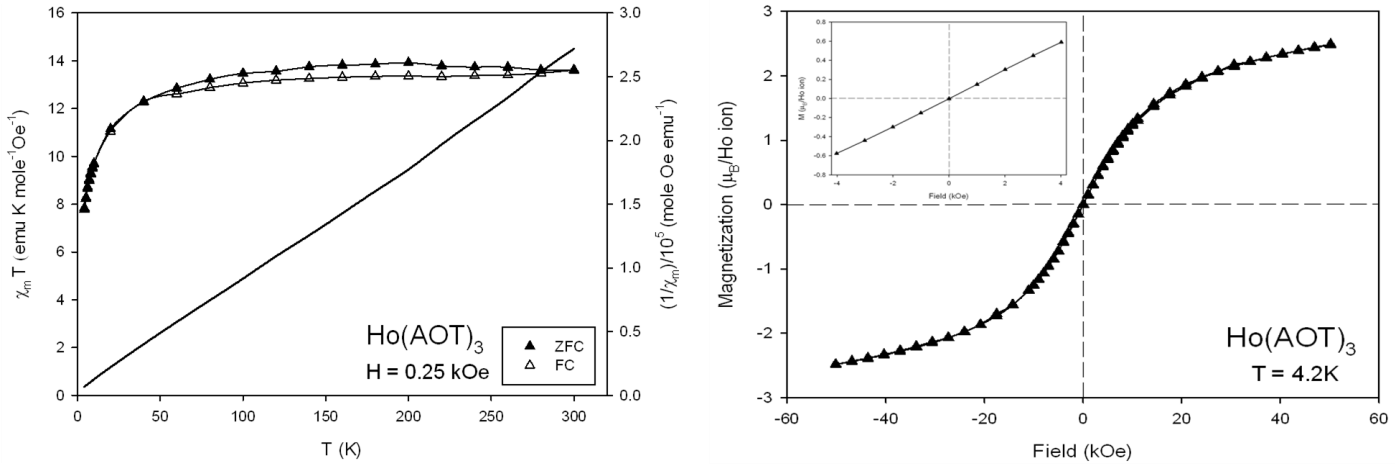

Figure S6d: SQUID magnetometry data for $Ho(AOT)_3$ showing **left**: temperature dependence of $\chi_m T$ and $1/\chi_m$ for each surfactant measured under 0.25 kOe; and **right**: magnetization versus applied magnetic field. The inset shows the detail of the low magnetic field region

References

1. K. Trickett, D. Xing, J. Eastoe, R. Enick, A. Mohamed, M.J. Hollamby, S. Cummings, S.E. Rogers, R.K. Heenan, *Langmuir* **2009,** *26*, 4732-4737.
2. J. Rogers, P.A.Winsor, *J. Coll. Int. Sci.* **1969,** *30*, 247-257.
3. R.K. Heenan, *Fish Data Analysis Program*; Rutherford Appleton Laboratory pp RAL, 1989.
4. (a) J.P. Hansen, J.B. Hayter, *Mol.Phys.* **1982,** *46*, 651 - 656; (b) J.B. Hayter, J. Penfold, *J. Coll. Polym. Sci.* **1983,** *261*, 1022; (c) J.B. Hayter, J. Penfold, J. *Coll. Polym. Sci.* **1983,** *261*, 1022-1030; (d) J.B. Hayter, J. Penfold, *Mol. Phys.* **1981,** *42*, 109 - 118.
5. M. Kotlarchyk, S.M. Ritzau, *J. Appl. Crystallogr.* **1991,** *24*, 753-758.

6. Z.X. Li, A. Weller, R.K. Thomas, A.R. Rennie, J.R.P. Webster, J. Penfold,R.K. Heenan, R. Cubitt, *J. Phys. Chem. B* **1999,** *103*, 10800-10806.
7. J. Eastoe, S. Stebbing, J. Dalton, R.K. Heenan, *Colloids Surf. A* **1996,** *119*, 123-131.
8. J. Eastoe, G. Fragneto, B.H. Robinson, T.F. Towey, R.K. Heenan, F.J. Leng, *J. Chem. Soc. Farad. Trans.* **1992,** *88*, 461-471.